PITTING AND POROUS LAYER FORMATION ON n-InP ANODES

C. O'Dwyer[†‡], D. N. Buckley[†‡], M. Serantoni[‡], D. Sutton[‡]
and S. B. Newcomb[‡*]

[†] *Department of Physics, University of Limerick, Ireland*
[‡] *Materials and Surface Science Institute, University of Limerick, Ireland*
[*] *present address Sonsam Ltd., Glebe Laboratories, Newport, Co. Tipperary, Ireland*

ABSTRACT

Surface pitting occurs when InP electrodes are anodized in KOH electrolytes at concentrations in the range 2 – 5 mol dm^{-3}. The process has been investigated using atomic force microscopy (AFM) and the results correlated with cross-sectional transmission electron microscopy (TEM) and electroanalytical measurements. AFM measurements show that pitting of the surface occurs and the density of pits is observed to increase with time under both potentiodynamic and potentiostatic conditions. This indicates a progressive pit nucleation process and implies that the development of porous domains beneath the surface is also progressive in nature. Evidence for this is seen in plan view TEM images in which individual domains are seen to be at different stages of development. Analysis of the cyclic voltammograms of InP electrodes in 5 mol dm^{-3} KOH indicates that, above a critical potential for pit formation, the anodic current is predominantly time dependent and there is little differential dependence of the current on potential. Thus, pores continue to grow with time when the potential is high enough to maintain depletion layer breakdown conditions.

INTRODUCTION

There is considerable interest in the electrochemical formation of porosity in semiconductors, from the point of view of fundamental understanding and because of their potential applications.[1-7] Much of the work has focused on pore formation in n-and p-type silicon but investigations of pore formation in III-V semiconductors such as GaAs[8-11] and InP[12-15] have also been reported. It has been suggested that controlled modulation of the pore diameter and pore growth direction in such structures could lead to photonic crystals with a photonic band gap in the near-infra red or visible region. Pore growth in semiconductors has been shown to be affected by electrolyte concentration[12,16,17] and substrate type[18], orientation[19] and doping density.[20] Considerable progress has been made in understanding the basic mechanisms of pore formation in silicon under electrochemical conditions. For silicon, several pore formation models have been proposed to account for the variety of observed pore types,[21-23] but only a limited number of investigations of the mechanism of pore formation in III-V semiconductors have been reported. We have recently reported[12] that both potentiodynamic and potentiostatic anodization in KOH electrolytes can result in the formation of a porous region below the surface of an InP electrode. The evidence strongly suggests that the porous layer structure arises from the

penetration of pits into the surface at particular points and pore propagation within the InP originating at these points and proceeding along the (100) direction.[24] The electrolyte within the porous structure is connected to the bulk electrolyte by a limited number of surface pits which form channels through a dense near-surface layer, thus providing a mechanism by which the porous layer can grow. Consequently, these channels play a critical role in the evolution of the porous structure.

This paper presents results of a detailed investigation of the pitting of the InP surface in aqueous KOH electrolytes under anodic conditions and discusses the role of these pits in the formation of the sub-surface porous region.

EXPERIMENTAL

The working electrode consisted of polished (100)-oriented monocrystalline sulfur doped n-InP with a carrier concentration of $\sim 3 \times 10^{18}$ cm^{-3}. An ohmic contact was made by alloying indium to the InP sample and the contact was isolated from the electrolyte by means of a suitable varnish. The electrode area was typically 0.2 cm^2. Anodization was carried out in aqueous KOH electrolytes with concentrations in the range 2 – 5 mol dm^{-3}. A conventional three electrode configuration was used employing a platinum counter electrode and saturated calomel reference electrode (SCE) to which all potentials are referenced. Prior to immersion in the electrolyte, the working electrode was dipped in a 3:1:1 H_2SO_4:H_2O_2:H_2O etchant and rinsed in deionized water. All of the electrochemical experiments were carried out at room temperature and in dark conditions.

A CH Instruments Model 650A Electrochemical Workstation interfaced to a Personal Computer (PC) was employed for cell parameter control and for data acquisition. Slices for cross-sectional microscopic analysis were prepared by thinning to electron transparency using standard focused ion beam milling procedures by means of a FEI 200 FIBSIMS workstation. The transmission electron microscopy (TEM) characterization was performed using a JEOL 2010 TEM operating at 200 kV. All AFM data was acquired using a Topometrix Explorer.

RESULTS AND DISCUSSION

Potentiodynamic Anodization

Fig. 1 shows linear sweep voltammograms of n-InP electrodes in KOH electrolytes of 2, 3 and 5 mol dm^{-3} concentration. The potential was scanned at a rate of 2.5 mV s^{-1} from 0.0 V to an upper potential E_u. At potentials less than 0.3 V, very little current flow is observed in each case, but continued anodization to potentials greater than 0.35 V results in a rapid increase in the current density. For example, in 5 mol dm^{-3} KOH (Fig. 1a) the current density increases rapidly from a value of 1 mA cm^{-2} at 0.35 V to a peak value of 20 mA cm^{-2} at 0.48 V. At potentials above the peak, the current density decreases quite rapidly, reaching a minimum value of 3 mA cm^{-2} at 0.6 V. Similar behavior is observed in 3 mol dm^{-3} and 2 mol dm^{-3} KOH (Figs. 1b and 1c) and a secondary peak is observed at higher potentials.

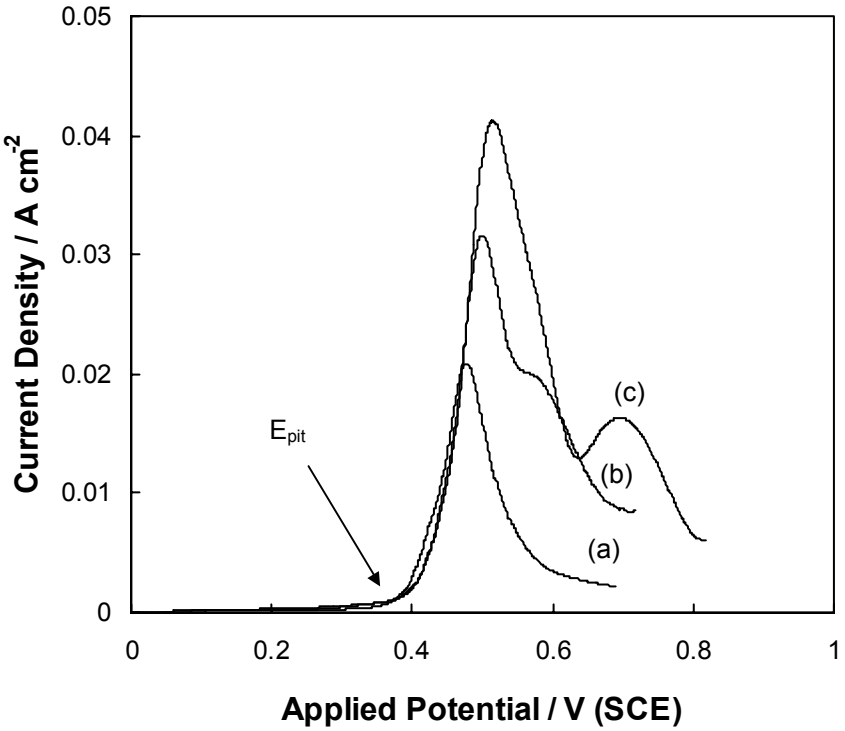

Fig. 1 Cyclic voltammograms n-InP electrodes in (a) 5 mol dm^{-3} (b) 3 mol dm^{-3} and (c) 2 mol dm^{-3} KOH. The potential was scanned at a rate of 2.5 mV s^{-1} from an initial potential of 0.0 V (SCE).

Visual inspection and optical microscopy of InP surfaces which were subjected to potential sweep anodization from 0.0 V to 0.35 V showed a specularly reflecting surface with very few features apparent. A typical AFM image of the surface after such a sweep in 5 mol dm^{-3} KOH is shown in Fig. 2a.

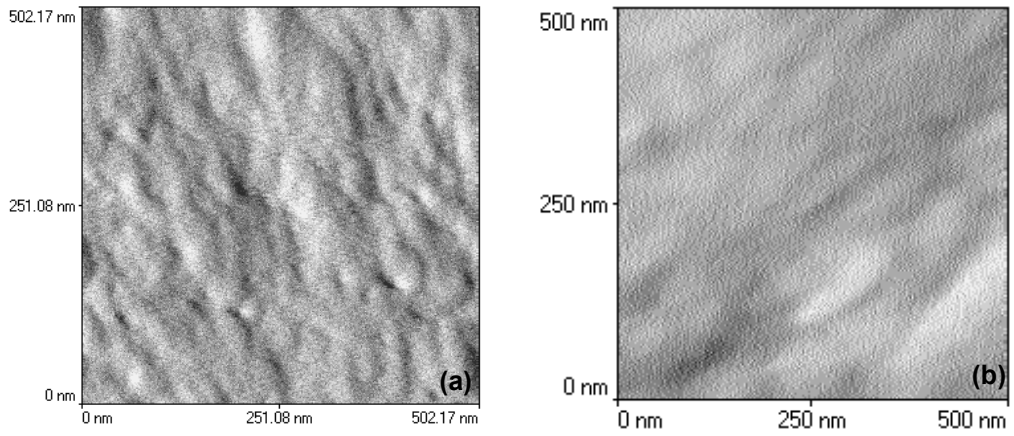

Fig. 2 AFM images of the surface of (a) an InP electrode after a potential sweep from 0.0 V to 0.3 V (SCE) in 5 mol dm^{-3} KOH at 2.5 mV s^{-1} and (b) an as-received InP wafer.

An image of a typical as-received InP wafer is shown for comparison in Fig. 2b. It is clear that anodization to this potential has caused relatively little surface modification. The root-mean-square (*rms*) roughness was estimated for both samples from the AFM data and values of 2.4 nm and 0.88 nm were obtained for the anodized and as-received samples respectively. Thus, anodization of InP electrodes to potentials of ~0.35 V results in some surface modification and a modest increase in roughness. However, there is no evidence of pit formation.

Fig. 3a shows an AFM image of the surface of an InP electrode that was subjected to a potential sweep from 0.0 V to 0.425 V in 5 mol dm^{-3} KOH at 2.5 mV s^{-1}. The image clearly shows an etch pit which has formed on the surface. Similar pits were observed in AFM images obtained for potential sweep experiments at other upper potentials in the range 0.4 V to 0.53 V. For example, an image obtained for an upper potential of 0.48 V (*i.e.* at the current peak) is shown in Fig. 3b. Line scans through the AFM images in Figs. 3a and 3b are shown in Figs. 3c and 3d. Although the AFM cannot measure the diameter of deep pits, we can obtain some estimate of the diameter of the pits from these traces. Thus, taking the value of the full width at half maximum (FWHM) from these traces we obtain a value of ~50 nm for the pit diameter in each case.

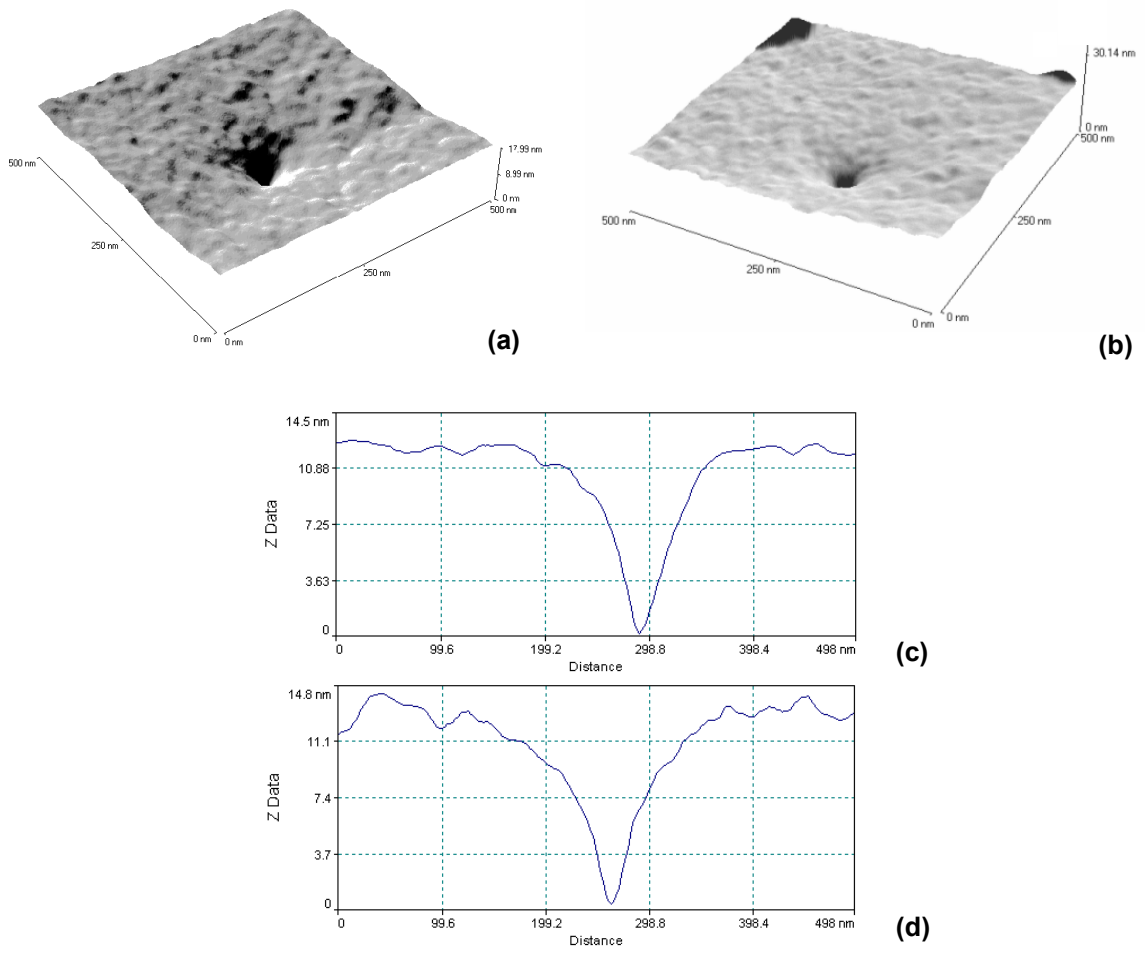

Fig. 3 AFM images of the InP surface after potential sweep anodization at 2.5 mV s^{-1} in 5 mol dm^{-3} KOH from 0.0 V to (a) 0.425 V, (b) 0.48 V. (c) Line scan of the pore shown in (a); (d) Line scan of the pore shown in (b).

Similar pits were observed in AFM images of InP electrodes subjected to potential sweep anodization in 2 mol dm^{-3} and 3 mol dm^{-3} KOH. The FWHM of the corresponding line scans suggest that the pit diameters are greater for 2 mol dm^{-3} KOH than for 3 mol dm^{-3} and 5 mol dm^{-3}. This would also correspond to the observation in TEM cross-sections of an increase in pore width as the KOH concentration is reduced.[12] Furthermore, for a given electrolyte concentration, the mean pit diameter, as determined from the FWHM of the AFM line scans through the centers of the pits, remains relatively constant.

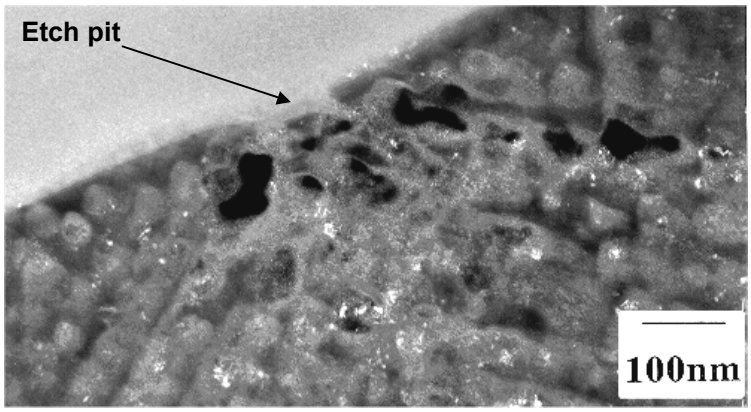

Fig. 4 Cross-sectional dark field TEM of an n-InP electrode after a potential sweep from 0.0 V to 0.675 V (SCE) in 3 mol dm^{-3} KOH at a scan rate of 2.5 mV s^{-1}. A channel through the near-surface layer is visible. The plane of the micrograph is (011).

TEM examination of electrode cross-sections also showed evidence of surface pits. A typical surface pit formed after a potential sweep in 3 mol dm^{-3} KOH from 0.0 V to 0.675 V is shown in Fig. 4. It can be seen that the surface pit extends through the near-surface layer forming a channel between the porous region of the substrate and the bulk electrolyte. The texture of this micrograph suggests that the pores emanate from the surface pits and there is evidence of increased levels of dissolution local to the surface pit.

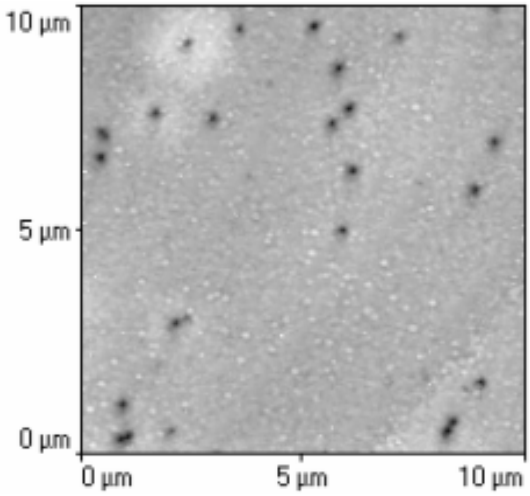

Fig. 5 AFM image of the surface of an InP electrode subjected to a potential sweep from 0.0 V to 0.48 V at 2.5 mV s^{-1} in 5 mol dm^{-3} KOH.

Estimates were made of the areal density of pits on electrode surfaces after anodization under potentiodynamic conditions. A series of experiments was carried out in which electrodes were subjected to potential sweeps at 2.5 mV s^{-1} from 0.0 V to upper potentials in the range 0.48 V to 0.68 V and 10 μm × 10 μm AFM images of the resulting surfaces were obtained. A typical such image is shown in Fig. 5 for an upper potential of 0.48 V (corresponding to the current peak). At this lower magnification, multiple pits are visible on the surface. By counting the pits (~23 for this image) in such images we can estimate the average areal density of pits in the surface.

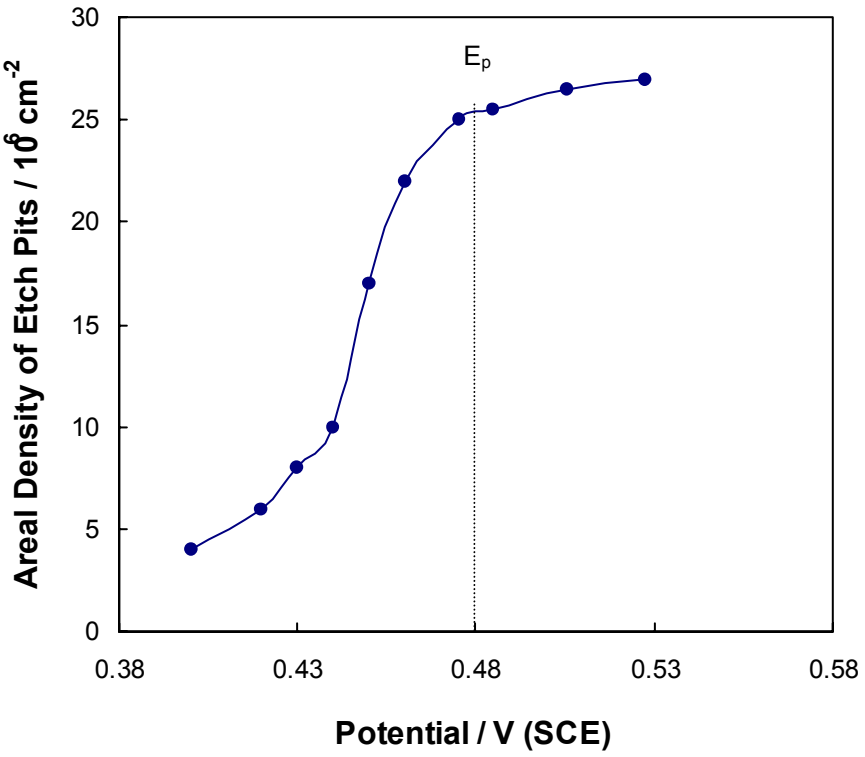

Fig. 6 Surface pit density, as determined by AFM, plotted as a function of the upper potential limit of the potential sweep. The scan rate was 2.5 mV s^{-1} and the electrolyte was 5 mol dm^{-3} KOH.

Estimates of pit density were similarly obtained for other upper potentials and the results are plotted in Fig. 6. It is clear that the density of pits in the surface increases progressively with increasing potential. The rate of increase is greatest in the vicinity of 0.45 V. This corresponds to half the peak current on the low-potential side of the peak in the current-voltage curve in Fig. 1a. Above ~0.48 V (*i.e.* the potential of peak current) the pit density begins to plateau and any further increase in pit density is small. Thus, the observed increase in density of pits in Fig. 6 corresponds to the onset of the anodic peak in Fig. 1a. There is evidence from TEM measurements[24] that a square based pyramidal porous domain forms beneath each etch pit on the surface. Thus, as the etch pits form progressively on the surface of the electrode, so the formation of porous domains also occurs progressively. The progressive formation of square-based pyramidal shaped porous domains beneath etch pits on the surface can be seen in the (100) plan view TEM images

in Fig. 7a. This plan-view TEM micrograph was acquired after ion-milling ~100 nm into the surface of an InP electrode subjected to a potential sweep from 0.0 V to 0.44 V in 5 mol dm^{-3} KOH at a scan rate of 2.5 mV s^{-1}. Numerous domains are visible and some are noted to be considerably more developed than others. Furthermore, in some areas, considerable domain merging has occurred. In Fig. 7b, a cross-sectional TEM of an electrode anodized under the same conditions is shown. This image was acquired from a region where domains are seen to merge. The image suggests that several pyramidal porous domains are overlapping. Also, a channel in the near-surface layer at the center of one of the overlapping pyramidal structures is evident at 'A' in Fig. 7b.

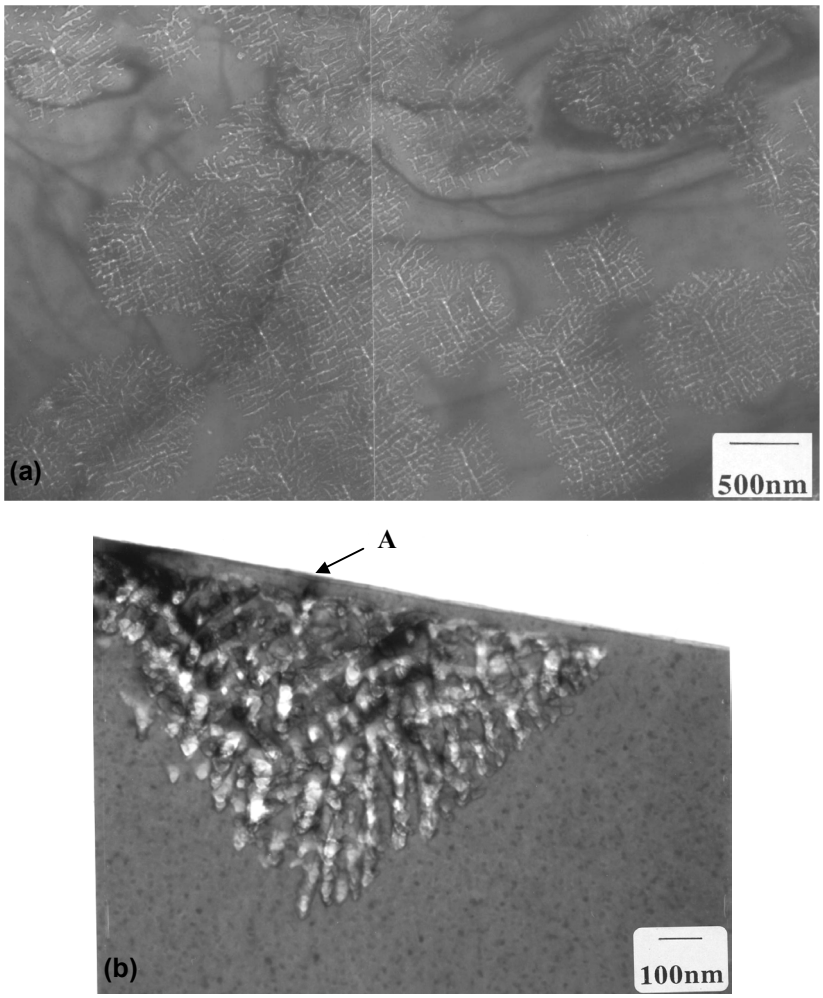

Fig. 7 (a) Plan view TEM of n-InP ~100 nm below the surface after a potential sweep from 0.0 V to 0.48 V at a scan rate of 2.5 mV s^{-1} in 5 mol dm^{-3} KOH electrolyte. The progressive development of the porous domains is apparent. (b) Cross-sectional (011) projection of the same electrode as in (a) showing merged pyramidal porous domains.

Potentiostatic Anodization

Experiments were also carried out at constant potential. In a series of experiments in 5 mol dm^{-3} KOH, the potential was stepped from open circuit to potential values in the range 0.5 – 0.75 V. These potentials correspond to values on a typical current-voltage

curve at which porous layer formation is observed. Fig. 8 shows the current-time curve obtained for an InP electrode anodized in 5 mol dm^{-3} KOH at a potential of 0.5 V. The current initially increases with time reaching a peak after 23 s and subsequently decreases. This type of current-time curve is typically observed where a nucleation process is occurring. Similar current-time curves are observed for InP electrodes anodized in 2 and 3 mol dm^{-3} KOH and details of these can be found elsewhere.[12] In all cases, porous layers are observed to form beneath the surface.

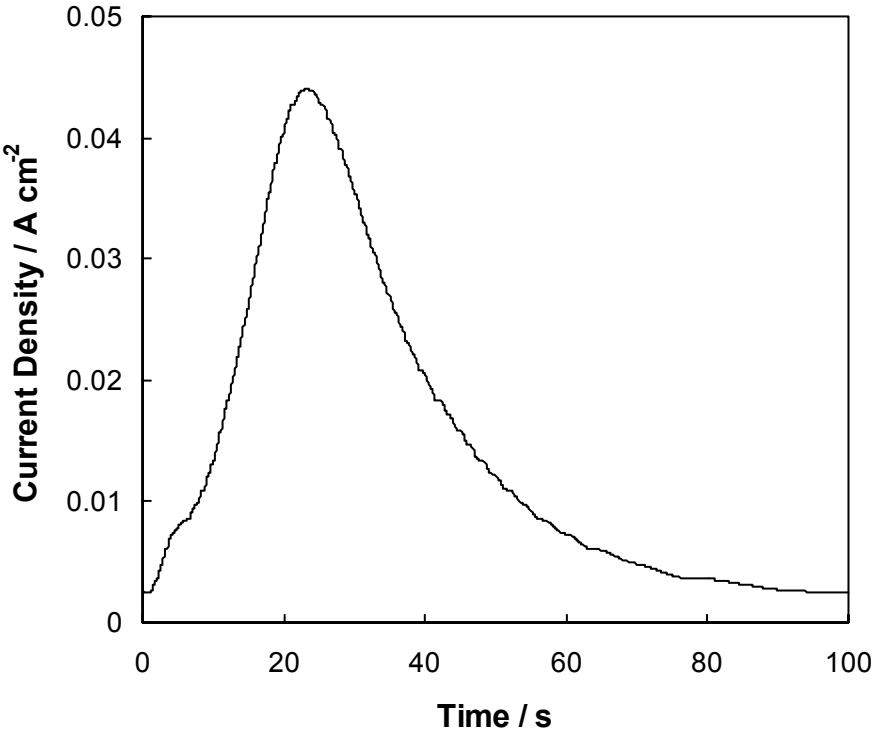

Fig. 8 Current-time curve for InP anodized at a potential of 0.5 V in 5 mol dm^{-3} KOH.

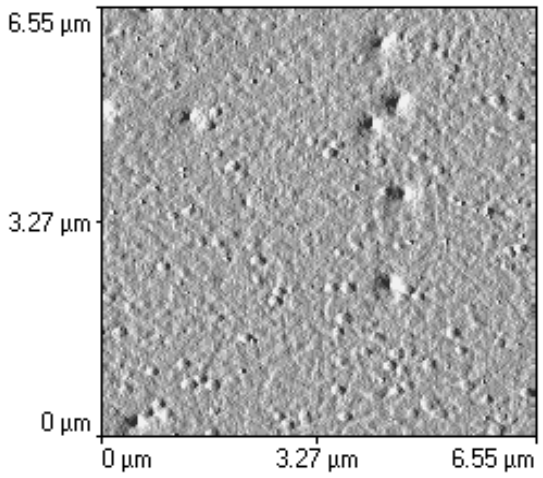

Fig. 9 AFM image of the InP surface after constant potential anodization at 0.5 V (SCE) in 5 mol dm^{-3} KOH for 25 s.

AFM studies were also conducted on electrode surfaces subjected to potentiostatic anodization. InP electrodes were anodized at 0.5 V for times ranging from 5 s to 40 s and AFM images of the surfaces were obtained. A typical image obtained after 25 s is shown in Fig. 9. Again, a pit similar to those shown in Figs. 3a and 3b can be observed. Images at other anodization times showed similar pits.

Values of pit density obtained from such images are plotted as a function of anodization time in Fig. 10. It is observed that the density of pits formed on the surface increases with time and approaches a plateau value after 20 – 30 s. Thus, surface pitting at constant potential develops in a similar manner to that observed under potential sweep conditions and is a progressive process.

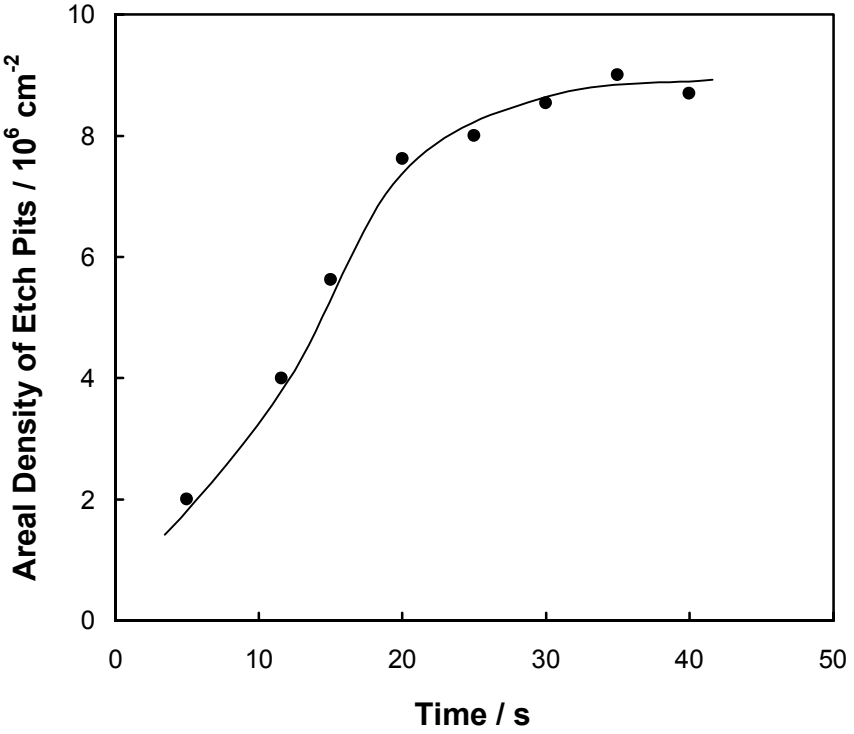

Fig. 10 Surface pit density plotted as a function of time. The data was acquired on multiple areas (10 μm × 10 μm) on multiple electrode surfaces anodized at 0.5 V in 5 mol dm^{-3} KOH.

Deconvolution of the Effect of Potential and Time

A series of cyclic voltammograms was obtained in which the potential was scanned from 0.0 V to higher values of the upper potential E_u at a scan rate of 2.5 mV s^{-1} in 5 mol dm^{-3} KOH. Typical cyclic voltammograms are shown in Fig. 11, where the upper potential E_u is less than the peak potential E_p. It is evident that an increase in current occurs initially on the reverse sweep as the potential is decreased, eventually reaching a current peak, after which the current decreases with decreasing potential.

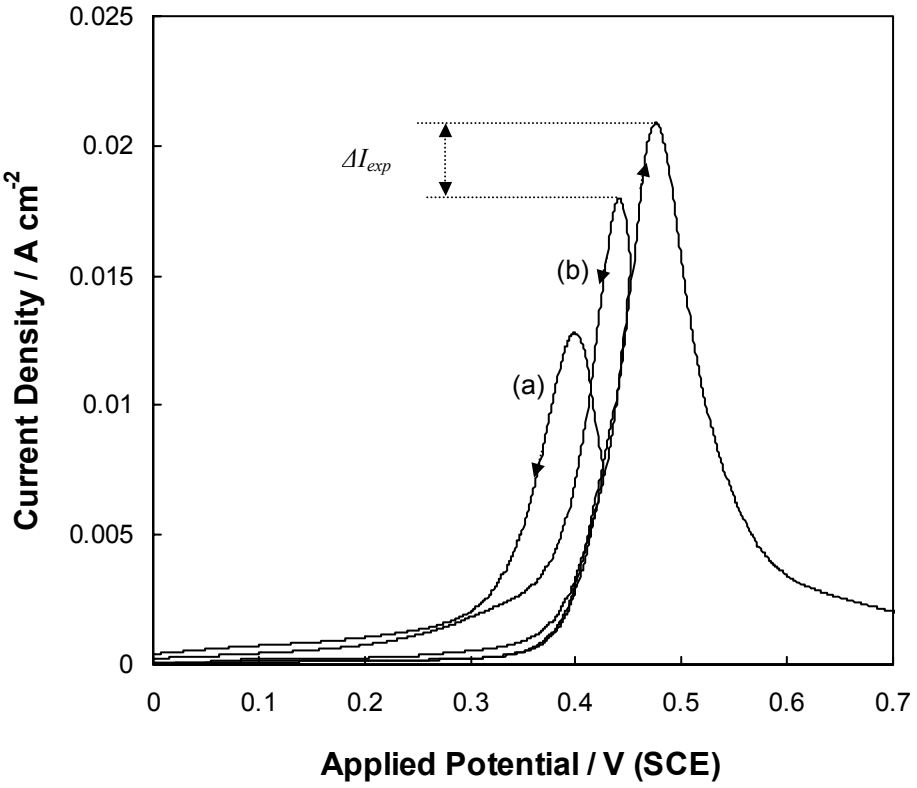

Fig. 11 Cyclic voltammograms of InP electrodes in 5 mol dm^{-3} KOH at a scan rate of 2.5 mV s^{-1} with upper potentials of (a) 0.445 V and (b) 0.47 V (SCE) respectively. ΔI_{exp} represents the difference in reverse scan peak current densities. A linear potential sweep from 0.0 V to 0.7 V at 2.5 mV s^{-1} is also shown.

Fig. 12 shows cyclic voltammograms of InP electrodes in 5 mol dm^{-3} KOH at a scan rate of 2.5 mV s^{-1} with upper potential limits greater than E_p. On the reverse scan, the current densities are lower than the corresponding current densities on the forward scan and continue to decrease as the potential is decreased. Cyclic voltammograms where $E_u = E_p$ show negligible hysteresis, *i.e.* the reverse curve coincides with the forward curve.

It is useful to examine the cyclic voltammograms in more detail to gain further insight into the temporal dependence of porous layer growth on InP under anodic conditions. As the measured current is a function of both potential E and time t, we can write

$$I = I(E,t) \tag{1}$$

Therefore,

$$dI = \left(\frac{\partial I}{dt}\right)_E dt + \left(\frac{\partial I}{\partial E}\right)_t dE \tag{2}$$

and since $E = \nu t$, where ν is the scan rate,

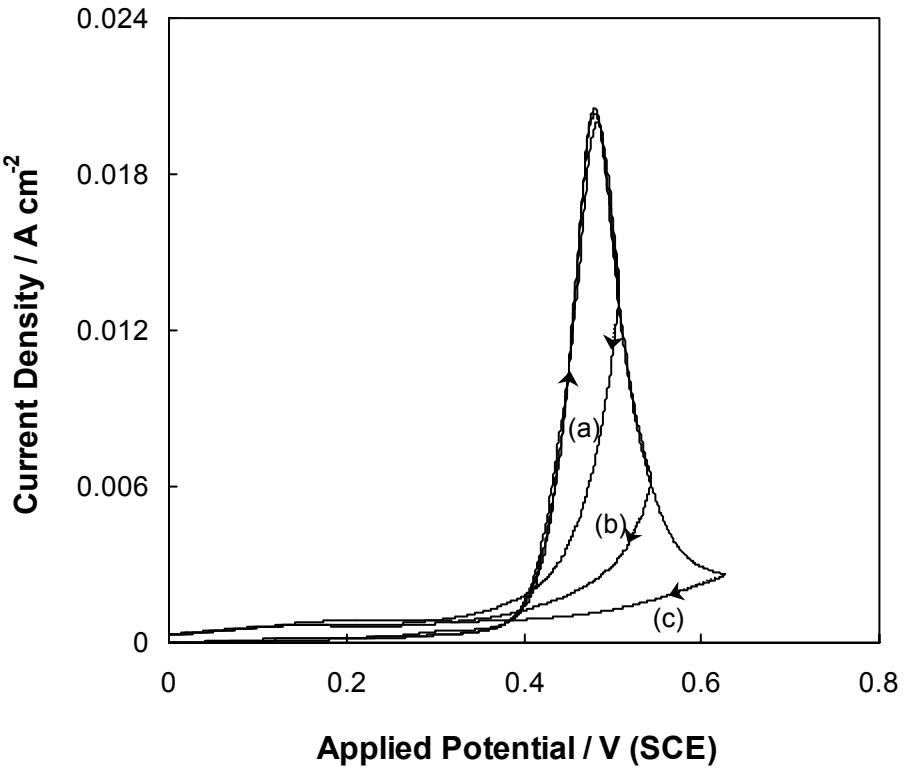

Fig. 12 Cyclic voltammograms of InP electrodes in 5 mol dm^{-3} KOH at a scan rate of 2.5 mV s^{-1} with upper potentials of (a) 0.52 V, (b) 0.55 V and (c) 0.65 V.

$$dI = \left(\frac{\partial I}{dt}\right)_E dt + \nu\left(\frac{\partial I}{\partial E}\right)_t dt \tag{3}$$

and

$$dI = \frac{1}{\nu}\left(\frac{\partial I}{\partial t}\right)_E dE + \left(\frac{\partial I}{\partial E}\right)_t dE \tag{4}$$

Thus, at any potential E_{exp} on a cyclic voltammogram, the slope of the forward curve is

$$\left(\frac{dI}{dE}\right)_{FWD,E_{\exp}} = \frac{1}{\nu}\left(\frac{\partial I}{\partial t}\right)_E + \left(\frac{\partial I}{\partial E}\right)_t \tag{5}$$

and the slope of the reverse curve is

$$\left(\frac{dI}{dE}\right)_{REV,E_{\exp}} = -\frac{1}{\nu}\left(\frac{\partial I}{\partial t}\right)_E + \left(\frac{\partial I}{\partial E}\right)_t \tag{6}$$

Although the functional relationship in Eqn. 1 is not necessarily the same for the forward and reverse curves, we assume that it is instantaneously the same at the point of potential reversal, *i.e.* at E_u. Thus it follows from Eqns. 5 and 6 that

$$\left(\frac{\partial I}{\partial E}\right)_t = \frac{\left(\frac{dI}{dE}\right)_{FWD,E_u} + \left(\frac{dI}{dE}\right)_{REV,E_u}}{2} = \frac{m_f + m_r}{2} \quad (7)$$

and

$$\left(\frac{\partial I}{\partial t}\right)_E = \frac{\nu\left\{\left(\frac{dI}{dE}\right)_{FWD,E_u} - \left(\frac{dI}{dE}\right)_{REV,E_u}\right\}}{2} = \frac{\nu\left(m_f - m_r\right)}{2} \quad (8)$$

where m_f and m_r are the slopes of the forward and reverse curves respectively at E_u. From cyclic voltammograms to various values of E_u in the range 0.41 – 0.626 V, the slope m_f of the forward curve at E_u and the slope m_r of the reverse curve at E_u were estimated. The values obtained are plotted in Fig. 13. The slope of the forward curve has the expected dependence for the derivative of the peak in the cyclic voltammogram, while the slope of the reverse curve is roughly equal and opposite in sign at all potentials.

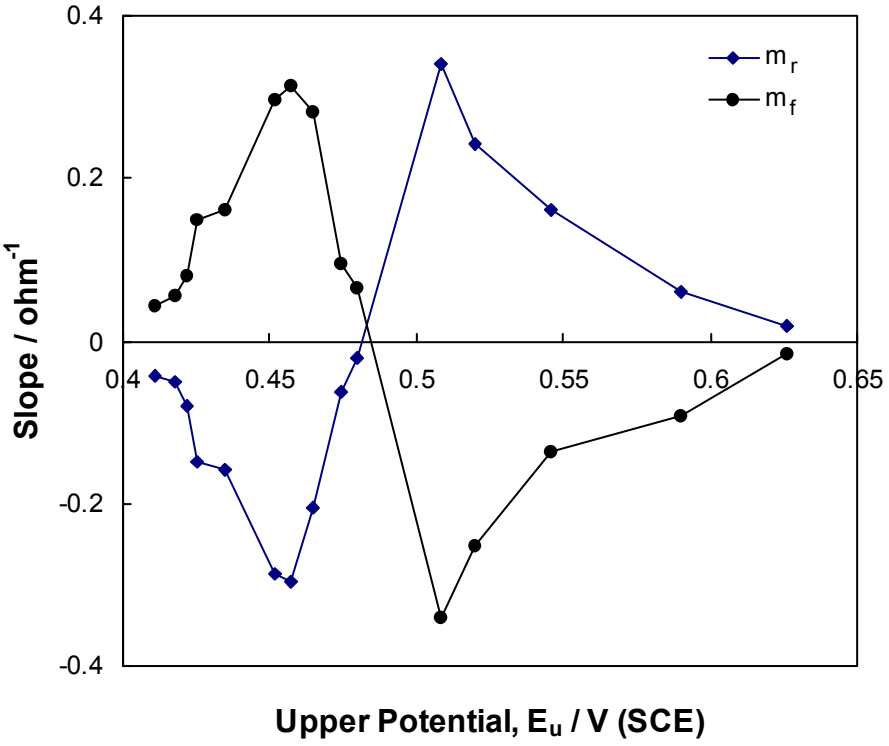

Fig. 13 Potential dependence of the slopes of the forward and reverse curves, m_f and m_r, at the upper potential limit E_u for a series of cyclic voltammograms of n-InP electrodes in 5 mol dm^{-3} KOH at a scan rate of 2.5 mV s^{-1}.

From the data in Fig. 13, $\left(\frac{\partial I}{\partial E}\right)_t$ and $\left(\frac{\partial I}{\partial t}\right)_E$ were estimated according to Eqns. 7 and 8 and the values obtained are plotted as a function of potential in Fig. 14. From Fig. 14, it can be seen that $\left(\frac{\partial I}{\partial E}\right)_t$ is small: the scale in Fig. 14 is the same as that in Fig. 13. Thus most of the current variation observed in the region of the anodic peak in the cyclic voltammogram is due to a time dependence rather than a true voltage dependence of the current.

It can also be seen from Fig. 14 that, at potentials less than 0.48 V (the potential of the current peak), the values of $\left(\frac{\partial I}{\partial t}\right)_E$ are positive indicating that current increases with time while at potentials greater than 0.48 V, the values of $\left(\frac{\partial I}{\partial t}\right)_E$ are negative indicating that current decreases with increasing time. This is explicable in terms of the mechanism of pore growth reported previously[24]. Once a critical potential for pit formation is reached, the increase in current (representing the growth of sub-surface pores) is primarily controlled by time. Initially, the current increases with time as surface pits are nucleated and each pit gives rise to a growing porous domain. After some time, domains begin to merge and eventually no longer grow: this gives rise to a decrease in current.

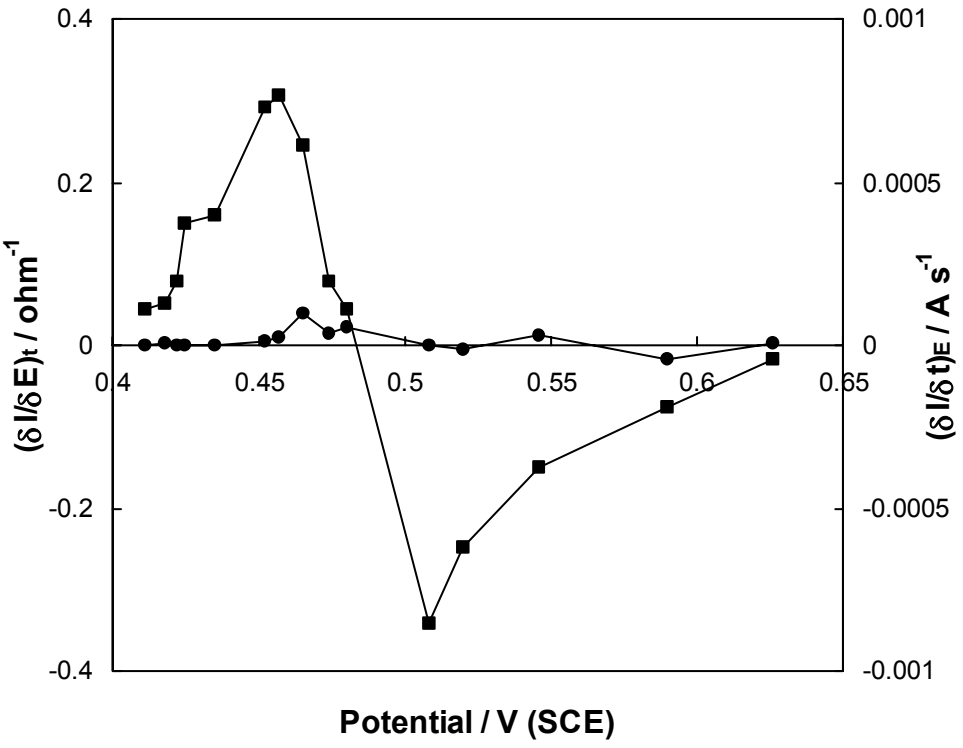

Fig. 14 Potential dependence of $\left(\frac{\partial I}{\partial E}\right)_t$ (-●-) and $\left(\frac{\partial I}{\partial t}\right)_E$ (-■-) at the upper potential limit E_u. The plot is derived from the data in Fig. 13.

Mechanism of Pit Initiation

For pitting of the surface to occur under anodic conditions, it has been suggested that a mechanism which limits current flow across the interface is essential to establish the conditions necessary for localized preferential etching.[25] This current limitation occurs either due to passivation of the surface or due to the absence of available holes at the surface of n-type semiconductors anodized in the dark. Breakdown of the depletion layer at more defective sites occurs at lower potentials[26,27] and enhanced dissolution will occur at these sites resulting in pitting.[28] A similar effect may occur due to breakdown of an otherwise stable oxide film on the surface.

Whether pit initiation stems from a breakdown mechanism within the semiconductor or breakdown of a surface film, the resulting effect is the same: pitting of the substrate occurs. Once a pit is formed, the electric field is greatly enhanced due to the curvature of the pit bottom. Thus, preferential hole generation occurs in the vicinity of the pit bottom leading to an enhanced etch rate.

CONCLUSIONS

Anodization of n-InP in a KOH electrolyte at concentrations of 2 mol dm^{-3} or greater results, under certain conditions, in selective etching of InP and the formation of a porous InP layer near the surface of the electrode. Linear sweep voltammograms of n-InP electrodes in these electrolytes show a pronounced anodic peak. AFM measurements show that pitting of the surface occurs both under potentiodynamic and potentiostatic conditions. The pits formed in 5 mol dm^{-3} KOH are observed to have a typical diameter of ~ 50 nm. Each of these pits acts as a source for a pyramidal porous domain, and these domains eventually merge to form a continuous porous layer. The density of surface pits is observed to increase with time under both potentiodynamic and potentiostatic conditions indicating a progressive pit nucleation process. This implies that the development of porous domains beneath the surface is also progressive in nature. Evidence for this is seen in plan view TEM images in which individual domains are seen to be at different stages of development. Analysis of the cyclic voltammograms of InP electrodes in 5 mol dm^{-3} KOH indicates that, above a critical potential for pit formation, the anodic current is predominantly time dependent and there is little differential dependence of the current on potential. Thus, pores continue to grow with time when the potential is high enough to generate a plentiful supply of holes at the pore tips, *i.e.* to maintain depletion layer breakdown conditions.

REFERENCES

[1] L.T. Canham, *Appl. Phys. Lett.*, **57**, 1046 (1990)
[2] H. Föll, *Appl. Phys. A*, **53**, 8 (1991)
[3] T. Holec, T. Chvojka, I. Jelínek, J. Jindřich, I. Němec, I. Pelant, J. Valenta and J. Dian, *Mater. Sci. Eng. C*, **19**, 251 (2002)
[4] R.J. Martín-Palma, J.M. Martínez-Duart, L. Li and R.A. Levy, *Mater. Sci. Eng. C,* **19**, 359 (2002)
[5] A. Matoussi, T. Boufaden, A. Missaoui, S. Guermazi, B. Bessaïs, Y. Mlik and B. El Jani, *Microelectronics Journal,* **32**, 995 (2001)
[6] A. Jain, S. Rogojevic, S. Ponoth, N. Agarwal, I. Matthew, W.N. Gill, P. Persans, M. Tomozawa, J.L. Plawsky and E. Simonyi, *Thin Solid Films,* **398**, 513 (2001)
[7] N.E. Chayen, E. Saridakis, R. El-Bahar, Y. Nemirovsky, *J. Molec. Biol.,* **312**, 591 (2001)
[8] S. Langa, J. Carstensen, M. Christophersen, H. Föll, and I.M. Tiginyanu, *Appl. Phys. Lett.*, **78**, 1074 (2001)
[9] G. Oskam, A. Natarajan, P.C. Searson and F.M. Ross, *Appl. Surf. Sci.*, **119**, 160 (1997)
[10] M.M. Faktor, D.G. Fiddyment and M.R. Taylor, *J. Electrochem. Soc.*, **122**, 1566 (1975)
[11] F.M. Ross, G. Oskam, P.C. Searson, J.M. Macaulay and J.A. Liddle, *Philos. Mag. A*, **75**, 2 (1997)
[12] C. O'Dwyer, D.N. Buckley, V.J. Cunnane, D. Sutton, M. Serantoni and S.B. Newcomb, in *Proceedings of the State-of-the-Art Program on Compound Semiconductors XXXVII*, PV 2002-14, p. 259, The Electrochemical Society, Proceedings Series, Pennington, NJ (2002)
[13] S. Langa, J. Carstensen, I.M. Tiginyanu, M. Christophersen and H. Föll, *Electrochem. Solid-State Lett.*, **4**, G50 (2001)
[14] S. Langa, I.M. Tiginyanu, J. Carstensen, M. Christophersen and H. Föll, *Electrochem. Solid-State Lett.* **3**, 514 (2000)
[15] E. Harvey, C. O'Dwyer, T. Melly, D.N. Buckley, V.J. Cunnane, D. Sutton, S.B. Newcomb and S.N.G. Chu, in *Proceedings of the 35th State-of-the-Art Program on Compound Semiconductors*, P.C. Chang, S.N.G. Chu, and D.N. Buckley, Editors, PV 2001-2, p. 87, The Electrochemical Society, Proceedings Series, Pennington, NJ (2001)
[16] P. Schmuki, J. Fraser, C.M. Vitus, M.J. Graham, H.S. Isaacs, *J. Electrochem. Soc.*, **143**, 3316 (1996)
[17] P. Schmuki, D.J. Lockwood, J. Fraser, M.J. Graham, H.S. Isaacs, *Mater. Res. Soc. Symp. Proc.,* **431**, 439 (1996)
[18] M. Christopherson, J. Carstensen, A. Feuerhake and H. Föll, *Mater. Sci. Eng. B*, **69**, 70, 194 (2000)
[19] S. Rönnebeck, J. Carstensen, S. Ottow and H. Föll, *Electrochem. Solid-State Lett.*, **2**, 126 (1999)
[20] P. Schmuki, L.E. Erickson, D.J. Lockwood, J.W. Fraser, G. Champion, H.J. Labbé, *Appl. Phys. Lett.*, **72,** 1039 (1998)
[21] B.H. Erne, D. Vanmaekelbergh and J.J. Kelly, *J. Electrochem. Soc.*, **143**, 305 (1996)
[22] J. Carstensen, M. Christophersen and H. Föll, *Mater. Sci. Eng., B*, **69-70**, 23 (2000)
[23] S. Langa, J. Carstensen, I.M. Tiginyanu, M. Christophersen and H. Föll, *Electrochem. Solid-State Lett.*, **5**, C14 (2002)

[24] C. O'Dwyer, D. N. Buckley, D. Sutton and S. B. Newcomb, in *Proceedings of the State-of-the-Art Program on Compound Semiconductors XXXVIII*, E.B. Stokes, R.C. Fitch, D.N. Buckley, P.C. Chang, Y. Koide, R.F. Kopf, F. Ren, R.E. Sah, P.H. Shen, and D.M. Walker, Editors, PV 2003-04, p. 63, The Electrochemical Society, Proceedings Series, Pennington, NJ (2003)
[25] I.E. Vermier, H.H. Goosens, F. Vanden Kerchove and W.B. Gomes, *J. Electrochem. Soc.*, **139**, 1389 (1992)
[26] A. Yammamoto and S. Yano, *J. Electrochem. Soc.*, **122**, 260 (1975)
[27] M.J. Theunissen, *J. Electrochem. Soc.*, **119**, 351 (1972)
[28] P. Schmuki, J. Fraser, C.M. Vitus, M.J. Graham and H.S. Isaacs, *J. Electrochem. Soc.*, **143**, 3316 (1996)